THE JOURNAL OF BIOLOGICAL CHEMISTRY VOL. 288, NO. 42, pp. 30125–30138, October 18, 2013

Evaluation of Cancer Dependence and Druggability of PRP4 Kinase Using Cellular, Biochemical, and Structural Approaches[S]

Received for publication, April 1, 2013, and in revised form, August 12, 2013 Published, JBC Papers in Press, September 3, 2013, DOI 10.1074/jbc.M113.473348

Qiang Gao[‡1], Ingrid Mechin[§1], Nayantara Kothari[‡], Zhuyan Guo[‡], Gejing Deng[‡], Kimberly Haas[¶], Jessica McManus[‡], Dietmar Hoffmann[‡], Anlai Wang[‡], Dmitri Wiederschain[‡], Jennifer Rocnik[‡], Werngard Czechtizky[‖], Xin Chen[¶], Larry McLean[¶], Heike Arlt[‡], David Harper[‡], Feng Liu[‡], Tahir Majid, Vinod Patel**, Christoph Lengauer[‡2], Carlos Garcia-Echeverria[‡], Bailin Zhang[‡], Hong Cheng[‡], Marion Dorsch[‡3], and Shih-Min A. Huang[‡4]**

*From [‡]Discovery and Early Development, Sanofi Oncology, Cambridge, Massachusetts 02139 and 94400 Vitry-sur-Seine Cedex, France, **Lead Generation and Candidate Realization, Sanofi, Waltham, Massachusetts 02451, [‖]Lead Generation and Candidate Realization, Sanofi, Industriepark Höchst, 65926 Frankfurt, Germany, [¶]Lead Generation and Candidate Realization, Sanofi, Bridgewater, New Jersey 08807, and [§]Tucson Research Center, Sanofi, Tucson, Arizona 85755*

Background: Little is known about the cancer dependence and druggability of PRP4.
Results: Significance of PRP4 catalytic activity is demonstrated, novel substrates are identified, and features of kinase domain structure are revealed.
Conclusion: PRP4 is required for cancer cell survival, displays substrate specificity, and is amenable to pharmacological inhibition.
Significance: Our results indicate that PRP4 is a potential drug target to pursue in cancer.

PRP4 kinase is known for its roles in regulating pre-mRNA splicing and beyond. Therefore, a wider spectrum of PRP4 kinase substrates could be expected. The role of PRP4 kinase in cancer is also yet to be fully elucidated. Attaining specific and potent PRP4 inhibitors would greatly facilitate the study of PRP4 biological function and its validation as a credible cancer target. In this report, we verified the requirement of enzymatic activity of PRP4 in regulating cancer cell growth and identified an array of potential novel substrates through orthogonal proteomics approaches. The ensuing effort in structural biology unveiled for the first time unique features of PRP4 kinase domain and its potential mode of interaction with a low molecular weight inhibitor. These results provide new and important information for further exploration of PRP4 kinase function in cancer.

PRP4 kinase was first identified from screens designed to isolate genes essential for pre-mRNA splicing processes in *Schizosaccharomyces pombe*. These studies revealed that mutations of fission yeast PRP4 kinase led to the accumulation of pre-mRNA species (1). Human PRP4 kinase (hPRP4)[5] encodes a 1007-amino acid protein containing an N-terminal 340 amino acid arginine/serine-rich domain (RS domain) commonly found in pre-mRNA splicing factors (2). Further investigation into the PRP4 protein complex has identified a diverse array of binding partners, including kinases, transcription factors, chromatin remodeling factors, deubiquitinases, and spindle checkpoint proteins, indicating additional potential biological functions (2–5). For example, it is recognized that PRP4 kinase functions in controlling mitosis. In fission yeast, the expression of dominant negative PRP4 protein leads to cell cycle arrest at both G_1/S and G_2/M (6). RNAi depletion of PRP4 kinase in *Drosophila melanogaster* has been shown to lead to a mitotic defect (7). Furthermore, using HeLa as a mammalian cell model, it was demonstrated that PRP4 loss of function resulted in spindle assembly checkpoint failure (4). Among the substrates identified for PRP4 kinase are splicing factors SF2, PRPF6, and PRPF31 as well as KLF13 and ELK-1 transcription factors that are involved in numerous cellular functions independent of splicing (5, 8–10). These findings suggest a broader spectrum of PRP4 functions than reported previously, thus meriting further biological investigation of this kinase as a potential therapeutic target for drug discovery.

The role for PRP4 kinase in cell growth control has been well documented in *S. pombe*, *Caenorhabditis elegans*, and human cancer cell lines. For example, it was shown that PRP4 kinase is essential for growth in fission yeast (11), and disruption of *C. elegans* PRP4 by RNAi resulted in a highly penetrant early embryonic lethality (3). In experiments utilizing siRNAs to screen for kinases essential for pancreatic cancer cell survival, PRP4 knockdown was demonstrated to increase apoptosis and decrease viability (12). In a genome-wide pooled shRNA screen, shRNAs against PRP4 were shown to reduce the viability of

[S] This article contains supplemental Tables 1–5.
The atomic coordinates and structure factors (codes 4IAN, 4IFC, 4IIR, and 4IJP) have been deposited in the Protein Data Bank (http://wwpdb.org/).
[1] Both authors contributed equally to this work.
[2] Present address: Blueprint Medicines, 215 First St., Cambridge, MA 02142.
[3] Present address: Agios Pharmaceuticals, 38 Sidney St., 2nd Fl., Cambridge, MA 02139.
[4] To whom correspondence should be addressed: Sanofi Oncology, 640 Memorial Dr., Cambridge, MA 02139. Tel.: 617-665-4934; E-mail: alex.huang@sanofi.com.
[5] The abbreviations used are: hPRP4, human PRP4 kinase; SILAC, stable isotope labeling with amino acids in cell culture; AIMS, accurate inclusion mass screening; Bis-Tris, 2-[bis(2-hydroxyethyl)amino]-2-(hydroxymethyl)propane-1,3-diol; MRM, multiple reaction monitoring; AMPPNP, adenosine 5′-(β,γ-imino)triphosphate; KD, kinase-dead; DYRK, dual specificity tyrosine phosphorylation-regulated kinase; CLK, cell division cycle-like kinase; SRPK, serine/arginine-rich protein kinase; Compound A, 4-{5-[(2-chloro-pyridin-4-ylmethyl)-carbamoyl]-thiophen-2-yl}-benzo[b]thiophene-2-carboxylic acid amine.

DLD-1, HCT-116, and HCC1954 cancer cell lines (13). Similarly, PRP4 kinase was identified as a potential therapeutic target in a pooled shRNA screen designed to identify genes required for proliferation and survival of diffuse large B-cell lymphoma cell lines (14). Moreover, in an effort to reveal potential kinase targets to treat multidrug-resistant ovarian cancer, inhibition of PRP4 activity by shRNAs was shown to resensitize chemoresistant human ovarian cancer to paclitaxel treatment (15). Interestingly, loss of PRP4 kinase was also demonstrated to enhance paclitaxel activity in breast cancer cells (16).

Taken together, the preceding observations indicate that targeting PRP4 kinase inhibition could be an attractive approach for targeted cancer therapy. However, the full repertoire of PRP4 substrates in cancer cells has not been fully elucidated, and the requirement for PRP4 kinase enzymatic activity *versus* its scaffolding function has not been formally investigated in the context of oncogenic dependence. Furthermore, no information currently exists regarding the structure of the PRP4 kinase domain, thus hindering rational design of potent and selective PRP4 inhibitors. In this report, we provide evidence that the kinase domain of PRP4 is essential for regulating cancer cell growth and survival. In addition, through a global proteomics approach, we expand the interactome and phosphoproteome of PRP4 kinase in cancer cells. These new findings not only identify suitable biomarkers to monitor PRP4 kinase activity but also provide interesting biological insights into the role of PRP4 cancer pathogenesis. Finally, we solve the x-ray structures of apo-PRP4, PRP4-ADP complex, PRP4-AMPPNP complex, and PRP4-inhibitor complex and identify several features suitable for rational design of PRP4 kinase inhibitors.

EXPERIMENTAL PROCEDURES

shRNA Sequences, Lentivirus Preparation, Cell Infection, and Viability Analysis—pSILENT9-eGFP, which drives expression of shRNA and enhanced GFP from the H1 promoter, was used to deliver shRNAs against PRP4. The shRNA sequences used were: 1) shRNA B, GGTAAGGCCAGATCTCCTACTGAT; 2) shRNA D, GCGAGTAGCTGCTGATGTTAA; and 3) shRNA E, GGAATCTTCGTCTGATGATAA. These shRNA-expressing lentiviral vectors were packaged in 293T cells using the Trans-Lentiviral packaging kit (Open Biosystems). Virus-containing media were collected, filtered, and concentrated by ultracentrifugation. Viral titers were measured by serial dilution on HT1080 cells followed by flow cytometric analysis after 48 h. HCT-116 and PANC-1 cells (Dulbecco's modified Eagle's medium (DMEM) + 10% FBS) were transduced with the pSILENT9 shRNAs at an multiplicity of infection of 5. The percentages of infected cells and viability were assessed by GFP expression and propidium iodide, respectively, using a FACSCalibur flow cytometer (BD Biosciences). The CELLQuest™ software (BD Biosciences) was used for data acquisition and analysis. For rescue experiments, PANC-1 cells stably expressing HA-tagged, shRNA-resistant PRP4 wild type and PRP4 kinase-dead were established with blasticidin selection (6 μg/ml) using the pLENTI9-IRES_BLASTR lentiviral expression system. Stable cell lines were then transduced with pSILENT9 shRNA D, and the cells were monitored for viability as described above.

Determination of Kinetic Activity of Recombinant PRP4 Proteins—The kinetic activity of PRP4 proteins was evaluated by performing an enzyme titration experiment using a microfluidic mobility shift assay. The enzymatic reaction was carried out at room temperature with 1 μM 5-fluo-ELK(412–423) (Abgent), a saturating concentration of ATP (2 mM), and varied concentrations of enzyme (2-fold dilution series from 128 to 4 nM) in an assay buffer containing 8 mM MOPS, pH 7.5, 10 mM $MgCl_2$, 0.015% Brij-35, 1 mM DTT, and 5% DMSO. Phosphorylation of ELK-1 peptide was monitored in kinetic mode using a LabChip EZ Reader II (Caliper Life Sciences). The assay was performed in a 384-well plate with a final volume of 80 μl.

Stable Isotope Labeling with Amino Acids in Cell Culture (SILAC) and Protein Preparation—PANC-1 cells harboring a doxycycline-inducible PRP4 shRNA construct were routinely cultured at 37 °C in a humidified atmosphere of 95% air and 5% CO_2 in DMEM supplemented with 10% fetal bovine serum. For SILAC experiments, PANC-1 cells were maintained in SILAC medium comprising L-lysine- and L-arginine-depleted DMEM (Thermo Scientific) supplemented with 10% dialyzed fetal bovine serum (Invitrogen), L-lysine and L-arginine (Invitrogen), or L-[$^{13}C_6$,$^{15}N_4$]arginine (Arg10) and L-[$^{13}C_6$,$^{15}N_2$]lysine (Lys8) added at a concentration of 0.1 g/liter for light or heavy stable isotope labeling. Both light and heavy isotope-labeled PANC-1 cells were maintained for at least eight doublings to achieve >95% incorporation of labeled amino acid. Then the heavy labeled PANC-1 cells were treated with doxycycline for 72 h, and the light labeled cells were treated with PBS as controls. Equal amounts of heavy labeled and light labeled cells were mixed, and the nuclear proteins were extracted with an NE-PER kit following the standard protocol provided by the vendor (Thermo Scientific). Proteins were denatured in 8 M guanidine and reduced/alkylated with 10 mM DTT and 10 mM iodoacetamide for 60 min followed by digestion with sequencing grade modified trypsin (1:25, w/w) (Promega) at 37 °C overnight. The digestion reaction was terminated by adding formic acid at a concentration of 0.1%.

Strong Cation Exchange Chromatography and Phosphopeptide Enrichment—Preparative chromatographic separations were performed on an Agilent 1200 HPLC system (Agilent) using a Poly-SULFOETHYL column (4.6 × 200 mm, 5-μm particle; PolyLC Inc.). 6 mg of desalted PANC-1 tryptic digest peptides was loaded in mobile phase A (10 mM ammonium formate, pH 3.0 in 25% acetonitrile). Mobile phase B consisted of 500 mM ammonium formate, pH 3 in 25% acetonitrile. Twenty 2-ml fractions were sequentially collected throughout the gradient. Each individual fraction was desalted and concentrated prior to phosphopeptide enrichment by solid phase extraction using Waters Oasis reversed-phase HLB cartridges (Waters). The eluted samples were lyophilized and reconstituted in a solution containing 80% acetonitrile with 2.5% TFA. The phosphopeptides were enriched using a TiO_2 affinity column (GL Sciences) following the manufacturer's procedure. The peptide mixture was incubated in the TiO_2 column for 30 min and washed twice with 0.3 M oxalic acid in 80% acetonitrile with 0.1% TFA. Finally, the phosphopeptides were eluted with 5% NH_4OH, and the eluents were dried in a SpeedVac (Thermo Fisher).

Mass Spectrometry Analysis and Data Interpretation—LC-tandem mass spectrometry (MS/MS) analysis was carried out on an LTQ OrbitrapVelos mass spectrometer (Thermo Scientific) equipped with a Thermo nanospray source (Thermo, San Jose, CA) and coupled with an Eksigent NanoLC Ultra 2D system (AB SCIEX). Separation of peptide mixtures was achieved on a 75-μm-inner diameter microcapillary trap column packed with 18 cm of Magic C_{18} resin (3 μm, 200 Å; Michrom Bioresources) with a gradient of acetonitrile (3–35%) in 0.1% formic acid for 145 min at a flow rate of 300 nl/min. A voltage of 3 kV was applied to generate electrospray. All the mass spectrometry (MS) and MS/MS spectra were acquired in the data-dependent mode. The full-scan spectra (peptide mass-to-charge ratios (m/z) from 300 to 1800) were acquired at resolution of 60,000 at m/z 400 with an accumulation target value of 1×10^6. The top 20 most intense ions at a threshold above 500 counts were selected for fragmentation by collision-induced dissociation at a normalized collision energy of 40%. Dynamic exclusion was applied to reject ions from repeated MS/MS selection for 90 ms using monoisotopic precursor selection. Singly charged ions with unassigned charge state were also excluded from MS/MS.

The mass spectrometry data were processed using Proteome Discoverer 1.3 (Thermo Scientific). The MS/MS peak lists were extracted and searched by Mascot against a concatenated forward and reversed version of the Swiss-Prot human database. The precursor and fragment mass tolerances were set to 10 ppm and 0.5 Da, respectively. Cysteine carbamidomethylation was searched as a fixed modification, whereas *N*-acetyl protein; *N*-pyroglutamine; oxidized methionine; phosphorylation of serine, threonine, and tyrosine; and SILAC labels on arginine and lysine were searched as variable modifications. The raw MS files were loaded to Proteome Discoverer 1.3, and peptides were quantified with the MSQuant software embedded in Proteome Discoverer. MSQuant calculated the ratio average over the peptide elution time, and the assignments used for quantification were visually displayed and validated. To minimize the false discovery rate, all phosphopeptide identifications were filtered by Mascot score. We accepted peptides based on the criterion that the number of forward hits in the database was at least 200-fold higher than the number of reversed database hits, which gives an estimated false discovery rate of less than 1% ($p < 0.01$). The final filtering criteria at which p was less than 0.01 were a peptide with Mascot score $\geq$20 and the peptide should be identified in the correct SILAC form (heavy or light) and contain the correct number of lysine and arginine residues specified by the mass difference observed in the full scan between the SILAC partners.

Verification of Candidate Kinase Substrates by Accurate Inclusion Mass Screening (AIMS)—Targeted mass spectrometry, specifically AIMS, was used for further verification. AIMS was performed on the LTQ-Orbitrap system described above with exactly the same LC condition. The created inclusion mass lists were exported in a comma-separated value format with separate columns for MS mass (m/z), start (min), end (min), and MS charge state. The files were imported into the global parent mass list to trigger collision-induced dissociation on themselves upon detection during MS1 acquisition with the matched accurate mass and charge states. Monoisotopic precursor selection was enabled, whereas non-peptide monoisotopic recognition was not enabled. Charge state rejection was enabled, and unassigned charge states and charge state 1 were rejected. Repeat count was set to 2. Exclusion mass width low was set to7.5 ppm, and exclusion mass width high was set to 7.5 ppm. Repeat duration was set to 15s; exclusion duration was set to 30s. The parent mass width was set to 7.5 ppm for both high and low m/z. No retention time prediction was associated with the given peptides during the experiments.

Immunoaffinity Purification of PRP4 Interaction Partners—Monoclonal anti-HA antibodies were covalently coupled to protein G-Sepharose beads (Roche Applied Science) at 2 mg/ml. The lysates were prepared by radioimmune precipitation assay buffer and incubated with anti-HA antibody overnight. After incubation, the Sepharose beads were washed three times with radioimmune precipitation assay buffer. To ensure efficient elution of bound proteins, a small aliquot of Laemmli buffer was added, and the solution was heated at 60 °C for 10 min. Eluted proteins were reduced by 10 mM DTT and alkylated by 50 mM iodoacetamide afterward. Proteins were separated on NuPAGE Novex 4–12% Bis-Tris gradient gels. Gels were Coomassie-stained for visualization. Then gels were destained overnight before excision of slices. After in-gel digestion with trypsin (Promega), the resulting peptides were extracted from the gel slices and stored for LC-MS/MS analysis.

Validation of PRP4 Substrate by Multiple Reaction Monitoring (MRM)—MRM analyses were performed on a system consisting of an Agilent 1290 binary pump (Agilent Technologies), a PAL HTC autosampler (LEAP Technologies), and an AB SCIEX AP5500 QTRAP mass spectrometer equipped with an electrospray ion source. The LC separation was carried out on a Waters HSS T3 C_{18} column (100 $\times$ 2.1 mm, 1.7 μm) at a flow rate of 300 μl/min. Water containing 0.1% (v/v) formic acid was used as eluent A, and acetonitrile containing 0.1% (v/v) acid formic was used as eluent B with a linear gradient from 5 to 60% B in 25 min and from 50 to 100% B in 3 min. MS/MS analysis was performed in positive ionization mode using an ion spray voltage of 5500 V. Analyst 1.4.2 software was used for the instrument control, data acquisition, and data processing. Data were acquired with both Q1 and Q3 at the unit resolution. The Turbo ion spray source was operated with the following parameters: 5.0-kV capillary voltage, 500 °C source temperature, 20-p.s.i. curtain gas, 35-p.s.i. GS1, and 40-p.s.i. GS2. For the final validation of PRP4 substrate candidates, peptide RDSPPPPAR from PAK4 (MRM transitions 538.5 $\rightarrow$ 865.3 and 538.5 $\rightarrow$ 213.2) was selected for the quantitative measurement as the assay readout. The collision energy, declustering potential, and collision cell exit potential were optimized for each chosen MRM transition by infusion of a standard peptide obtained from chemical synthesis. The MRM transitions were monitored and acquired with a dwell time of 50 ms to ensure 25 and 30 data points per chromatographic peak.

Validation of PRP4 Substrate Phosphorylation and Measurement of Compound A Potency against PRP4 in Biochemical Assay—The PRP4 phosphorylation reaction was performed at room temperature with 15 nM full-length His-tagged PAK4 recombinant protein expressed in *Escherichia coli* (from American Research Products, Inc.), saturating concentration of ATP (2 mM), and 2.3 nM PRP4 enzyme kinase domain in an assay

buffer containing 8 mM MOPS, pH 7.5, 10 mM $MgCl_2$, and 1 mM DTT in a total volume of 100 μl for 1 h. Samples with PAK4 protein in reaction buffer alone without the presence of PRP4 kinase and PAK4 protein with PRP4 kinase-dead mutant were used as negative controls. For measuring Compound A potency against PRP4 using PAK4 as substrate, Compound A ranging from 0.5 nM to 1 μM was preincubated with PRP4 for 30 min at room temperature before the reaction was initiated with PAK4 protein substrate. Compound dilution (3-fold) was prepared in 100% DMSO and diluted 1:100 into the final reaction. After a 60-min incubation at room temperature, the reaction was terminated with formic acid (1% final). Phosphorylation of Ser^{104} in PAK4 was quantified by mass spectrometry as described above. IC_{50} was calculated by fitting data to a four-parameter logistic equation.

PRP4 Kinase Domain Expression and Purification for Structural Studies—pFastBac1 vector containing hPRP4(Asp^{657}–Ile^{1007})-His_6 was used to transform DH10Bac *E. coli* competent cells (Invitrogen) following the Invitrogen Bac-to-Bac protocol. Colonies confirmed to contain the recombinant plasmid were used for bacmid DNA isolation. Following PCR analysis, bacmid DNA from one of these colonies was used to transfect Sf9 cells and generate P1, P2, and P3 viral stocks. Titer of the P3 viral stock was determined to be 8.0×10^7 infectious units/ml. This was used to infect 2 liters of Sf9 insect cell culture at 1.0×10^6 cells/ml for 72 h at a multiplicity of infection of 5. Cells were then harvested by centrifugation (20 min at 4000 rpm), and the pellet was washed in 1× PBS buffer prior to a second round of centrifugation. The cell pellet was then stored at −80 °C for later use. All purification steps were performed at 4 °C. The cell pellet was thawed prior to addition of buffer A (50 mM Tris-HCl, pH 8.0, 200 mM NaCl, 30 mM imidazole, and 5 mM β-mercaptoethanol) and sonication. The lysate was centrifuged at 30,000 rpm for 35 min, and the supernatant was filtered before being loaded onto a 5-ml HisTrap nickel column (GE Healthcare) equilibrated with buffer A. The column was then washed with 10% buffer B (50 mM Tris-HCl, pH 8.0, 200 mM NaCl, 500 mM imidazole, and 5 mM β-mercaptoethanol) prior to applying a gradient from 10 to 100% buffer B. Fractions containing pure PRP4 were pooled together and concentrated prior to being loaded onto a gel filtration column equilibrated with final buffer (20 mM Tris-HCl, pH 8.0, 200 mM NaCl, and 5 mM tris(2-carboxyethyl)phosphine) to exchange the buffer and polish the protein. Two peaks corresponding to tetrameric and monomeric highly pure PRP4, respectively, were collected separately. Both samples were amenable to crystallization under the same conditions.

Crystallization, Data Collection, Refinement, and Model Building— hPRP4 in 20 mM Tris-HCl, pH8.0, 200 mM NaCl, and 5 mM tris(2-carboxyethyl)phosphine was then concentrated down to about 8 mg/ml for crystallization. Thin plate-shaped crystals can be easily obtained by vapor diffusion (hanging drop or sitting drop techniques) in a variety of conditions involving high molecular weight PEG and salt as additive for pH ranging from 6.5 to 8.5 at both 4 and 18 °C. We typically grew reproducible crystals by mixing an equal volume of protein solution with well solution composed of 0.2 M ammonium sulfate, 20–30% PEG 3350, and 0.1 M HEPES, pH 7.0 at 18 °C in the presence or absence of ligand. Crystals were cryoprotected by addition of glycerol or PEG 400. For the reported complexes of PRP4 with ADP, AMPPNP, and Compound A, apo crystals were soaked for longer times in cryoprotectant solution in the presence of 5 mM ligand (final concentration). Data sets were collected at 100 K using at Advanced Photon Source LS-CAT beamlines 21-ID-D and 21-ID-F (equipped with MAR300 CCD MARMosaic 225 detectors, respectively) and processed using HKL2000 by Shamrock Structures, LLC (17). For all data sets, Matthews coefficient calculation (18) using matthews_coef (19) in CCP4i (20, 21) established the presence of two molecules per asymmetric unit. Phasing of the apo data set was performed by molecular replacement in Phaser (22) using CLK2 (Protein Data Bank code 3NR9) as molecular replacement attempts using the closest analog, apo-DYRK2 (Protein Data Bank code 3K2L), failed to give a reasonable solution using both Phaser and AMoRe (23). Subsequent structures were solved using apo-PRP4 as the starting point. Model building was done using Coot (24). Refinement was carried out using CNX (25) with NCS constraints released in the last refinement cycles (apo) or BUSTER (all complexes) (26). The final coordinates for all discussed structures have been deposited in the Brookhaven Protein Data Bank with accession codes 4IAN, 4IFC, 4IIR, and 4IJP.

RESULTS

Kinase Activity of PRP4 Is Required for Maintaining Cancer Cell Viability—To verify the previously reported role of PRP4 in the regulation of cancer cell viability, we utilized three shRNAs (shRNAs B, D, and E) to knock down the endogenous expression of PRP4 in PANC-1 (pancreas) and HCT-116 (colorectal) tumor cell lines (12, 13). As illustrated in Fig. 1*A*, all three shRNAs significantly down-regulated endogenous PRP4 protein levels (*panels i* and *iii*) and reduced cell viability in both cancer cell lines (*panels ii* and *iv*). To rule out potential off-target effects of RNAi and to investigate the requirement of PRP4 kinase activity for the maintenance of oncogenic phenotype, we performed a rescue experiment utilizing shRNA-resistant wild-type PRP4 or its kinase-dead (KD) mutant (K717A). Results obtained from an *in vitro* biochemical assay using ELK-1 peptide as a substrate confirmed that PRP4 kinase-dead mutant lacks enzymatic activity (Fig. 1*B*) (10). Upon co-expression of PRP4-WT or PRP4-KD with PRP4 shRNA D in PANC-1 cells, PRP4 protein levels were clearly maintained in both PANC-PRP4-WT and PANC-PRP4-KD cell lines (Fig. 1*C*). However, only the expression of shRNA-resistant PRP4-WT, but not the KD mutant, restored the viability of PANC-1 cells following PRP4 knockdown (Fig. 1*D*). These results provide conclusive evidence that the effect of PRP4 shRNA D on growth inhibition is likely on-target and that the kinase activity of PRP4 is required to maintain tumor cell viability.

Identification of PRP4 Substrates through Global Proteomics Profiling—To gain further insight into the biological functions of PRP4 and to identify potential physiologically relevant substrates of PRP4 kinase activity, we first surveyed PRP4-associated protein complexes to establish a comprehensive view of the PRP4 interactome. In parallel, we initiated a SILAC-based quantitative global phosphoproteomics profiling experiment and confirmed the resulting candidate list using an AIMS

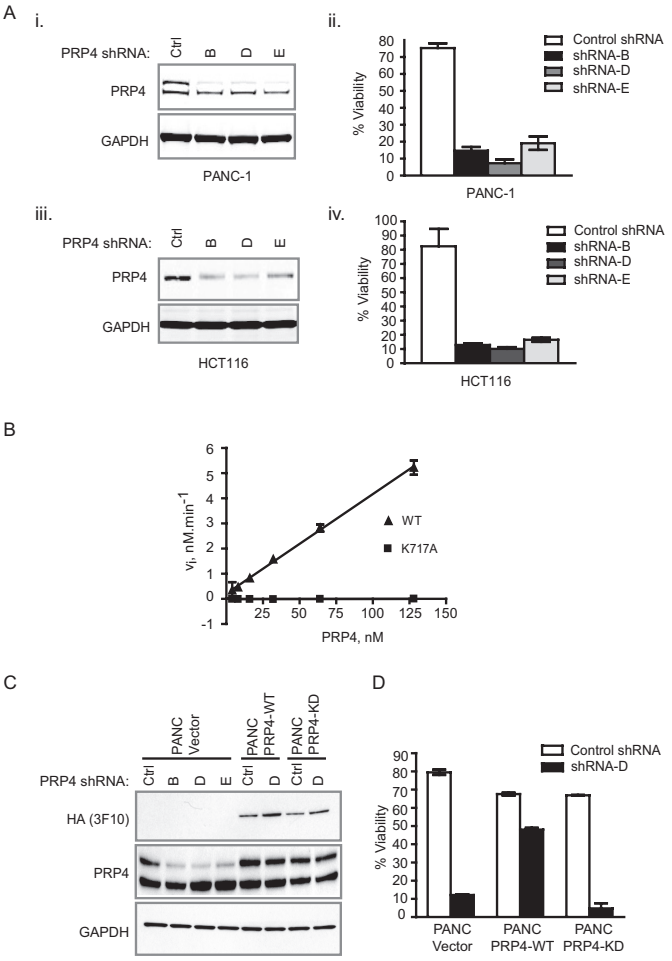

FIGURE 1. **Kinase activity of PRP4 is required for maintaining cell viability.** *A*, PRP4 knockdown by three independent shRNAs inhibits the viability of PANC-1 and HCT-116 cells. Depletion of endogenous PRP4 by three independent shRNAs in PANC-1 and HCT-116 cells was determined by Western blot (*panels i* and *iii*). *Panels ii* and *iv* denote the effect of control (*Ctrl*) shRNA and PRP4 shRNAs on cell viability. *B*, comparison of kinetic activity of recombinant PRP4-WT and PRP4-K717A of hPRP4(Val^{498}–Ile^{1007})-His$_6$. The initial velocity at each enzyme concentration was determined under the conditions described under "Experimental Procedures." Standard deviation was calculated and is shown as *error bars*. *C*, exogenous expression of shRNA D-resistant PRP4 cDNA restored the PRP4 protein levels upon PRP4 knockdown by shRNA. *D*, expression of shRNA-resistant PRP4-WT restored the viability of cells after PRP4 knockdown, whereas the expression of shRNA-resistant PRP4-KD did not.

approach. PRP4 binders revealed from the interactome studies were then cross-referenced with the data obtained from the phosphoproteomics profiling effort, resulting in the identification of high confidence novel substrates of PRP4 kinase. These results enabled us to develop both cell-based and biochemical assays to reliably monitor PRP4 enzymatic activity (Fig. 2*A*).

To carry out the PRP4 global interactome experiment, we first generated a doxycycline-inducible construct expressing HA-tagged hPRP4 and stably integrated it into the HEK293 Flp-In^{TM} cell line (Invitrogen) to generate a HEK293-FlpIn-HA-PRP4 cell line. Upon addition of doxycycline, the expression of HA-PRP4 was robustly induced (Fig. 2*B*). PRP4 was immunoprecipitated with immobilized HA antibody and subjected to LC-MS/MS (Fig. 2*C*). A total of 1022 proteins that interacted with PRP4 were identified (see supplemental Table 1). GeneGo analysis revealed that PRP4-associated complexes were significantly enriched in proteins involved in mRNA processing and cell cycle regulation, consistent with the previously reported functions of PRP4 (Fig. 2*D*) (27).

For the SILAC-based quantitative phosphoproteomics profiling, PANC-1 cells harboring a doxycycline-inducible PRP4 shRNA D construct (PANC-PRP4-shD) were passaged in media containing isotopically "heavy" [$^{13}C_6$,$^{15}N_2$]lysine/[$^{13}C_6$,$^{15}N_4$]arginine or "light" natural amino acids for several generations to achieve >95% labeling. The heavy and light cells were then treated with and without doxycycline, respectively, to trigger PRP4 knockdown and for control conditions (Fig. 3*A*). After 72 h of doxycycline induction, the PRP4 protein level was significantly diminished (Fig. 3*B*). Because PRP4 has previously been demonstrated to localize in the nucleus (2–4), we focused our profiling effort on nuclear extracts (Fig. 3*A*). To ensure that alterations observed in the phosphopeptide abundance were not the consequence of changes in total protein expression, we analyzed the total nuclear protein expression by gel electrophoresis-LC-MS (supplemental Table 2) and incorporated this information into subsequent analyses (28). A total of 2519 unique phosphopeptides representing 902 proteins were identified as a result of the SILAC-based phosphoproteomics profiling (supplemental Table 3). Of this total, 246 phosphopeptides from 209 proteins were significantly down-regulated, whereas total protein expression remained unchanged after depletion of endogenous PRP4 kinase (Fig. 3*C* and supplemental Table 4). A representative example of the identified spectrum for PAK4 is shown in Fig. 3*D*.

To examine the existence of a PRP4 consensus motif, we analyzed a 13-amino acid sequence surrounding the central phosphorylated residue with Motif-X software for the phosphopeptides that were down-regulated more than 2-fold (29). We found that the consensus sequence for PRP4 kinase was significantly overrepresented by the following motifs: *XXS*PXX* and *XXS*XXE*XX* (where *X* is any amino acid and S* and E* are phosphoacceptors). According to the NetworKIN algorithm (30), the Ser-Pro could also represent the consensus motif for MARK1 or CDK1 kinase (Fig. 3*E*, *panel i*). However, the -Ser-*X*-*X*-Glu sequence was identified as a novel motif and could be unique to PRP4 kinase (Fig. 3*E*, *panel ii*).

To further validate candidates obtained from SILAC-based phosphoproteomics profiling, we performed AIMS in the Orbitrap MS system. Data for *m*/*z* and charge state were collected based on a user-defined inclusion list, which consists of 153 phosphopeptides selected based on the -fold change and the reliability of the peptides identified from the prior global phosphoproteomics profiling experiment. We performed multiple AIMS replicates on the enriched phosphopeptides and summed the total ion chromatogram for each peptide across replicates. As a result, 29 phosphopeptides that were consistently down-regulated in both AIMS (+doxycycline/−doxycycline ratio ≤0.6) and SILAC methods were identified; albeit the extent of down-regulation for each phosphopeptide varied between the two methods (Table 1).

Assuming that proteins that exhibit decreased phosphorylation in the absence of PRP4 and are also present in the PRP4 complexes have a higher probability of being physiological substrates of PRP4 kinase, we cross-referenced the PRP4 interac-

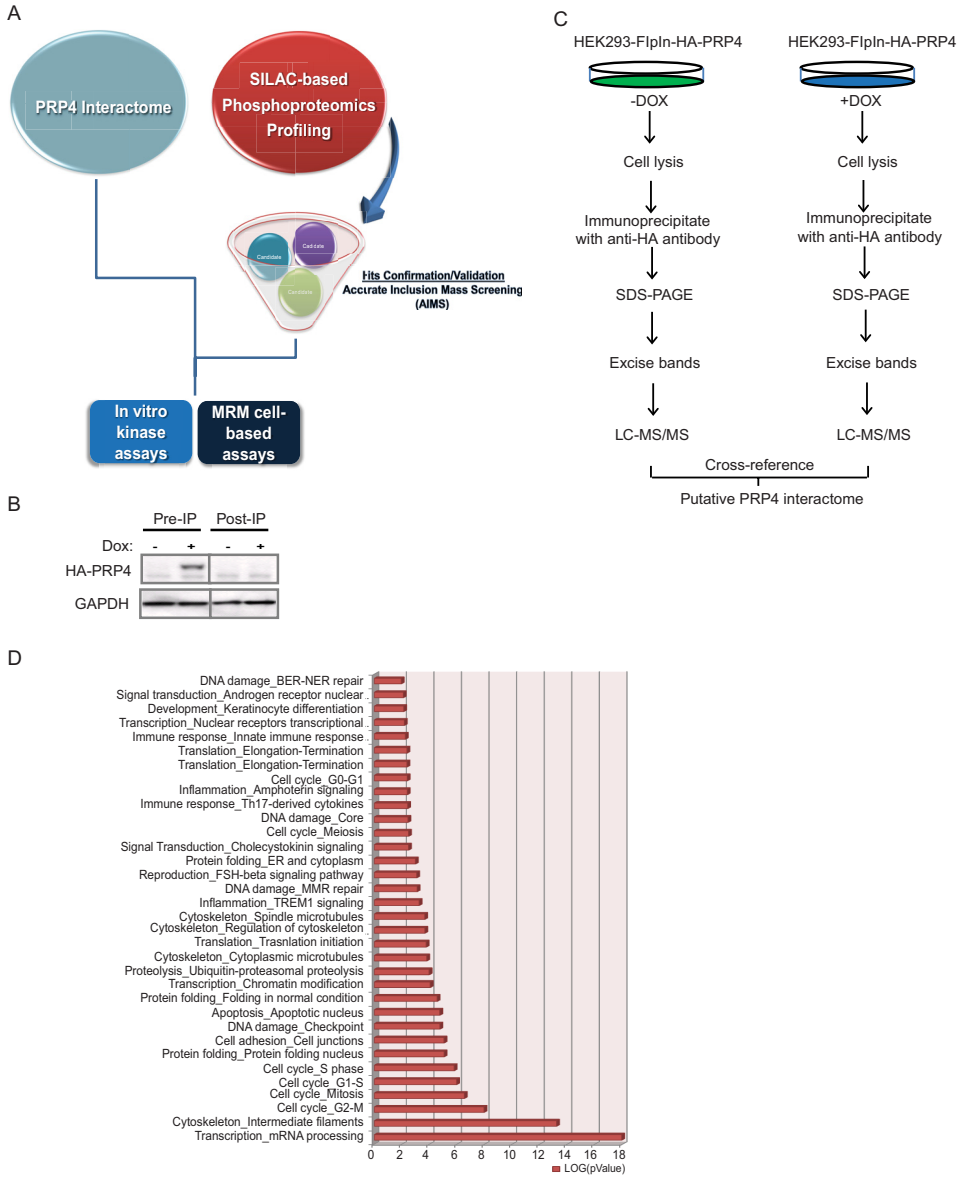

FIGURE 2. **The PRP4 interactome.** *A*, PRP4 substrate hunting strategy. PRP4 interactome was characterized by LC-MS/MS with the assumption that PRP4 substrates should be physically associated with PRP4. In parallel, a SILAC-based phosphoproteomics profiling experiment coupled with inducible knockdown of PRP4 was performed, and results were validated by AIMS. The interactome data were cross-referenced with the AIMS data to narrow down the candidate list. MRM-based mass spectrometry and PRP4 *in vitro* kinase assays were utilized to further validate the selected PRP4 substrate. *B*, successful depletion of exogenously expressed HA-tagged PRP4 by immunoprecipitation (*IP*) with anti-HA antibody. *C*, immunoprecipitation-MS workflow for characterization of PRP4 interactome. Exogenous expression of HA-tagged PRP4 kinase was induced by addition of doxycycline (*DOX*) and immunoprecipitated by the anti-HA antibody after lysis. The PRP4-associated proteins were separated by SDS-PAGE followed by in-gel digestion and mass spectrometry identification. For control, an identical experiment was performed using lysates without the induced expression of HA-PRP4. *D*, functional classification of PRP4 binding partners using GeneGo software based on universal gene ontology annotation terms. The top six functional categories are enriched with proteins associated with mRNA processing and cell cycle regulation. All categories presented in the graph have p values ≤0.01. *BER-NER*, base excision repair-nucleotide excision repair; *ER*, endoplasmic reticulum; *MMR*, mismatch repair.

tome with the candidate list shown in Table 1 and narrowed down the potential substrates to 12 phosphopeptides representing 12 different proteins (Table 1, highlighted in red). The phosphorylation intensity of some of these phosphopeptides was dramatically down-regulated by more than 80% following PRP4 knockdown.

Among the candidate PRP4 substrates were Arg/Ser-rich proteins with functions in pre-mRNA splicing, represented by SRSF6, SRRM2, and SF1. This is in accordance with the known function of PRP4 kinase. In addition, we uncovered several novel candidates, such as DNA replication licensing factor MCM2, elongation factor EEF1D, and nucleoprotein TPR, the phosphorylation status of which was dramatically down-regulated upon PRP4 depletion. TPR has been shown to directly bind to MAD1/MAD2, and its depletion has been shown to result in a marked decreased of MAD1 at the kinetochore and a defect in mitotic spindle check point (31). These observations are in stark resemblance to phenotypes observed in PRP4-depleted cells in which the disappearance of MAD1 from the kinetochore and the mitotic check point defect were evident (4). Interestingly, the phosphorylation of PAK4, a kinase that has previously been demonstrated to be

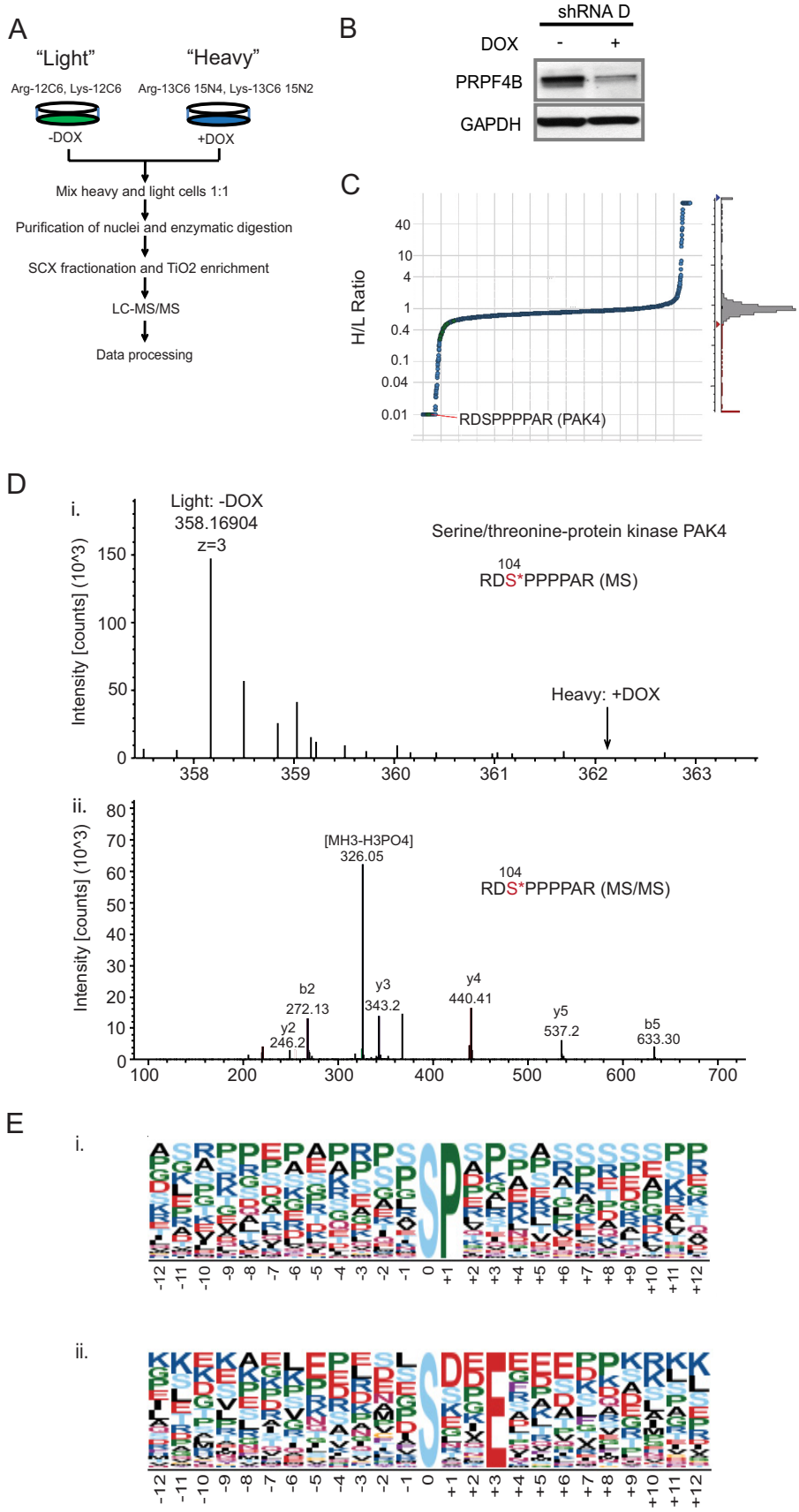
A
"Light"
"Heavy"
Arg-12C6, Lys-12C6
Arg-13C6 15N4, Lys-13C6 15N2
-DOX
+DOX
Mix heavy and light cells 1:1
Purification of nuclei and enzymatic digestion
SCX fractionation and TiO2 enrichment
LC-MS/MS
Data processing
B
shRNA D
DOX
-
+
PRPF4B
GAPDH
C
H/L Ratio
40
10
4
1
0.4
0.1
0.04
0.01
RDSPPPPAR (PAK4)
D
i.
Light: -DOX
358.16904
z=3
Serine/threonine-protein kinase PAK4
104
RDS*PPPPAR (MS)
Heavy: +DOX
Intensity [counts] (10^3)
ii.
[MH3-H3PO4]
326.05
104
RDS*PPPPAR (MS/MS)
b2
272.13
y2
246.2
y3
343.2
y4
440.41
y5
537.2
b5
633.30
E
i.
ii.

TABLE 1

Summary of phosphopeptides that were significantly down-regulated in SILAC-based phosphoproteomics profiling and confirmed by AIMS

An asterisk (*) indicates sites of phosphorylation. p-Peptide; phosphopeptide; DOX, doxycycline.

					AIMS peptide intensity		
Accession number	Protein name	Gene id	p-Peptide sequence	Modified site	-DOX	+DOX	Ratio (+DOX/-DOX)
O96013	Serine/threonine-protein kinase PAK 4	PAK4	RDS*PPPPAR	S104	27111106	166541	0.01
Q13247	Serine/arginine-rich splicing factor 6	SRSF6	SNS*PLPVPPSK	S303	3286876	1669015	0.51
Q15637	Splicing factor 1	SF1	TGDLGIPPNPEDRS*PS*PEPYNSEGKR	S80/S82	78279318	38819117	0.50
Q5VTR2	E3 ubiquitin-protein ligase BRE1A	RNF20	ALVVPEPEPDSDS*NQER	S138	604292	277662	0.46
Q9UQ35	Serine/arginine repetitive matrix protein 2	SRRM2	HGGS*PQPLATTPLSQEPVNPPSEASPTR	S377	6893361	2022765	0.29
Q96I25	Splicing factor 45	SF45	RPDPDS*DEDEDYER	S155	756122	208812	0.28
Q92785	Zinc finger protein ubi-d4	DPF2	VDDDS*LGEFPVTNSR	S142	1248665	708330	0.57
P49736	DNA replication licensing factor MCM2	MCM2	RRGNDPLTSS*PGR	S27	9080465	518162	0.06
Q9Y6M1	Insulin-like growth factor 2 mRNA-binding protein 2	IGF2BP2	ISYIPDEEVSSPS*PPQR	S164	1400205	600137	0.43
P10644	cAMP-dependent protein kinase type I-alpha regulatory subunit	PRKAR1A	EDES*PPPPNPVVK	S83	1421737	631569	0.44
Q92610	Zinc finger protein 592	ZNF592	DLSGPTKESSKGS*PK	S322	867825	29648	0.03
Q9Y618	Nuclear receptor corepressor 2	NCOR2	ANAS*PQKPLDLK	S956	135475	under detection limit	-
P61978	Heterogeneous nuclear ribonucleoprotein K	HNRNPK	IILDLISES*PIK	S216	2248	under detection limit	-
P29692	Elongation factor 1-delta	EEF1D	KPATPAEDDEDDDIDLFGS*DNEEEDKEAAQLR	S162	2870839	under detection limit	-
Q09666	Neuroblast differentiation-associated protein AHNAK	AHNAK	DIDISS*PEFK	S177	4688587	926135	0.20
Q8WXI9	Transcriptional repressor p66-beta	GATAD2B	GRLT*PS*PDIMLSDNEASSFR	S122	712391	55381	0.08
Q14247	Src substrate cortactin	CTTN	AKTQT*PPVSPARQPTEER	S405	554547	24344	0.04
Q8NYF8	Bcl-2-associated transcription factor 1	BCLAF1	KETQS*PEQVKSEK	S512	349837	18505	0.05
Q13200	26S proteasome non-ATPase regulatory subunit 2	PSMD2	DKAPVQPQQS*PAAAPGGTDEKPSGK	S16	1883412	189511	0.10
Q9UHR4	Brain-specific angiogenesis inhibitor 1-associated protein 2-like protein 1	BAIAP2L1	TPASTPVSGT*PQAS*PMER	S261	1108587	173702	0.16
Q96B97	SH3 domain-containing kinase-binding protein 1	SH3KBP1	ANS*PSLFGTEGKPK	S587	584590	96894	0.17
Q4KMP7	TBC1 domain family member 10B	TBC1D10B	AAGGAPS*PPPPVR	S403	2113816	274747	0.13
Q8WXE1	ATR-interacting protein	ATRIP	LAAPSVSHVS*PR	S224	1576272	843301	0.53
P08621	U1 small nuclear ribonucleoprotein 70 kDa	SNRNP70	YDERPGPS*PLPHR	S226	5729256	163750	0.03
P12270	Nucleoprotein TPR	TPR	TDGFAEAIHS*PQVAGVPR	S2155	579293	under detection limit	-
Q5VUA4	Zinc finger protein 318	ZNF318	IPS*PNLLK	S2101	901567	16914	0.02
Q13283	Ras GTPase-activating protein-binding protein 1	G3BP1	SSS*PAPADLAQTVQEDLR	S232	37594973	12868953	0.34
P61284	60S ribosomal protein L12	RPL12	IGPLGLS*PK	S38	409748	243914	0.60
Q13428	Treacle protein	TCOF1	LGAGEGGEASVS*PEK	S1378	9337251	1555407	0.17

important in both tumorigenesis and metastasis (32), was also significantly reduced at the Ser^{104} site after the knockdown of PRP4.

Based on these findings, we set out to establish a cellular assay to monitor PRP4 kinase activity using an MRM approach (33). MRM is known to be highly quantitative, sensitive, reproducible, and scalable to a high throughput screening format. To this end, we chemically synthesized PAK4 phosphopeptides and used two transitions for each peptide to develop an MRM assay (see "Experimental Procedures"). The nuclear extracts were prepared from doxycycline-induced or non-induced PANC-PRP4-shD cell line and digested with trypsin. The phosphopeptides were enriched by TiO_2 beads and subjected to MRM analysis. The results demonstrated that phosphorylation of PAK4 on Ser^{104} is decreased by ~3-fold after PRP4 depletion (Fig. 4, *A* and *B*). These results are consistent with our prior observation in global phosphoproteomics profiling and AIMS, thus further reinforcing the validity of aforementioned proteins as potential PRP4 substrates.

To strengthen our observations using PRP4-depleted cell extracts, we carried out *in vitro* biochemical kinase assays, which provide a more defined experimental setting. PAK4 was selected for the kinase assay validation because of the commercial availability of the full-length recombinant proteins. Briefly, PAK4 recombinant protein was incubated with the purified kinase domain of either PRP4-WT or PRP4-K717A mutant. The phosphorylated PAK4 was digested by trypsin and analyzed by mass spectrometry. As shown in Fig. 4*C*, the phosphorylation of PAK4 (Ser^{104}) was dramatically up-regulated in the presence of PRP4-WT but not of PRP4-K717A mutant. Notably, no other phosphorylation sites on PAK4 showed a similar trend (Fig. 4*D*), strongly demonstrating the specificity of PRP4 kinase for PAK4 Ser^{104}.

Unique Features of the X-ray Crystal Structure of PRP4 Kinase Domain—To provide the framework for future rational design of potent and selective PRP4 inhibitors, we purified the PRP4 catalytic domain and solved the x-ray structures of apo-PRP4, PRP4-ADP complex, PRP4-AMPPNP complex, and PRP4-inhibitor complex.

The apo data set resolution is 2.44 Å, and its space group is C2 with cell parameters $a = 73.27$ Å, $b = 75.29$ Å, $c = 148.00$ Å, $\alpha = \gamma = 90°$, and $\beta = 97°$. ADP, AMPPNP, and Compound A complex data sets were processed in P1 space group with cell parameters around $a = b = 52$ Å, $c = 79$ Å, $\alpha = 103°$, $\beta = 105°$, and $\gamma = 93°$ and set to 2.13-, 2.00-, and 2.25-Å resolution, respectively.

Table 2 summarizes the data collection and refinement statistics. A few regions on the PRP4 construct could not be built in any of our models due to the lack of electron density. These include the initial 12–14 amino acids at the N terminus, loops

FIGURE 3. **SILAC-based phosphoproteomics profiling for PRP4 substrate identification.** *A*, SILAC experiment flowchart. PANC-1 cells with a doxycycline (*DOX*)-inducible PRP4 shRNA construct stably integrated were divided into two populations and grown in light or heavy medium. Cells cultured in heavy medium were treated with doxycycline for 72 h to induce knockdown of endogenous PRP4, whereas those cultured in light medium were left untreated. Both batches of cells were combined in a ratio of 1:1 followed by nuclear protein extraction, protein digestion, affinity enrichment of phosphopeptides by strong cation exchange chromatography and a TiO_2 tip, and LC-MS/MS analysis. Data generated were processed by Proteome Discovery software. *B*, depletion of endogenous PRP4 by inducible PRP4 shRNA 72 h after doxycycline treatment. *C*, PRP4 depletion resulted in significant down-regulation of certain phosphopeptides. Most of the identified phosphopeptides maintained an intensity ratio of heavy/light close to 1, indicating minimal changes in phosphorylation. However, some were significantly down-regulated after induced knockdown of PRP4. Depicted herein is a phosphopeptide of PAK4 kinase. *D*, *panels i* and *ii*, examples of MS and MS/MS spectra of RDS*PPPPAR phosphopeptide of PAK4 kinase identified in SILAC-based phosphoproteomics profiling. *E*, *panels i* and *ii*, Motif-X analysis identified two over-represented motifs in the PRP4 substrate candidate list. All phosphopeptides with >2-fold down-regulation in phosphorylation intensity were analyzed. Motifs *XXS*P*XX* and *XXS*XXE*XX* were significantly overrepresented ($p < 10^{-6}$) according to the Motif-X algorithm.

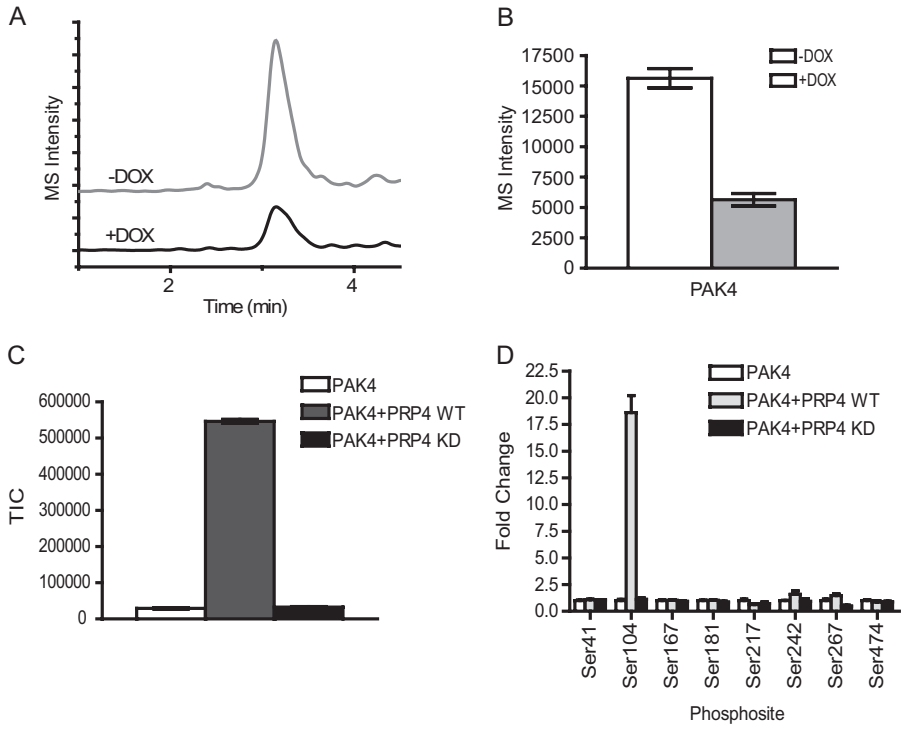

FIGURE 4. **Validation of PRP4 substrates by MRM cell-based assay and *in vitro* kinase assay.** *A*, extracted ion chromatograms of MRM spectra of transitions (538.5/865.3) monitored for the peptide RDS*PPPPAR of PAK4. An overlay of extracted ion chromatograms of the peptide from control cells without doxycycline treatment (*upper panel*) and cells with doxycycline (*DOX*) treatment (*lower panel*) are shown. *B*, the Ser^{104} phosphorylation of PAK4 was decreased by ~3-fold after induced PRP4 knockdown. Three biological replicates were performed, and the intensities of PAK4 peptide RDS*PPPPAR were averaged and plotted as a bar graph. *C*, PAK4 kinase can be phosphorylated by recombinant PRP4 *in vitro*. The *in vitro* kinase assay was performed as described under "Experimental Procedures." The resulting reaction mixture was digested by trypsin, and the peptide RDS*PPPPAR from recombinant PAK4 was identified and monitored by Orbitrap. The phosphorylation of the Ser^{104} residue of PAK4 was significantly increased by PRP4-WT recombinant protein (*gray bar*) but not by PRP4-KD (*black bar*). *D*, survey of all detectable phosphorylated sites in recombinant PAK4 showed that only the phosphorylation of Ser^{104} residue of PAK4 was significantly up-regulated by PRP4-WT. Standard deviation was calculated and is shown as *error bars*. *TIC*, total ion chromatogram.

TABLE 2

Summary of data collection and refinement statistics for crystal structures

Numbers in parentheses refer to statistics for the outer resolution shell. CpdA, Compound A; r.m.s.d., root mean square deviation; AU, asymmetric unit.

	Apo-PRP4	PRP4 + ADP	PRP4 + AMPPNP	PRP4 + CpdA
Protein Data Bank code	4IAN	4IFC	4IIR	4IJP
Data collection statistics[a]				
Space group	C2	P1	P1	P1
Cell parameters (length (*a*, *b*, *c*), Å; angle (α, β, γ), °)	$a = 73.27$, $b = 75.29$, $c = 148.00$, $\beta = 97.21$	$a = 52.32$, $b = 52.26$, $c = 78.98$, $\alpha = 104.47$, $\beta = 104.63$, $\gamma = 93.01$	$a = b = 52.50$, $c = 78.79$, $\alpha = 105.29$, $\beta = 103.05$, $\gamma = 93.090$	$a = 52.14$, $b = 52.54$, $c = 79.13$, $\alpha = 102.56$, $\beta = 105.250$, $\gamma = 92.29$
Resolution (Å)	50.00-2.44 (2.53-2.44)	50.00-2.15 (2.23-2.15)	50.00-2.00 (2.07-2.00)	50.00-2.25 (2.33-2.25)
Unique reflections	29,966 (2,836)	42,262 (4,162)	51,485 (5,095)	36,692 (3,636)
Redundancy	3.7 (3.1)	2.2 (2.2)	2.2 (2.2)	2.3 (2.3)
R_{merge} (%)	10.9 (53.3)	5.2 (39.5)	5.5 (38.4)	5.1 (42.7)
$I/\sigma I$	11.4 (2.3)	15.4 (2.1)	11.91 (2.2)	17.3 (2.3)
Completeness (%)	99.3 (93.5)	97.9 (97.2)	97.5 (97.0)	98.4 (97.5)
Refinement statistics[b]				
Resolution (Å)	47.91-2.44	31.04-2.15	26.16-2.00	47.61-2.25
R_{work}	23.6	25.0	25.3	25.9
R_{free}	23.7	26.7	28.2	27.4
r.m.s.d. bond distance (Å)	0.006	0.008	0.008	0.008
r.m.s.d. bond angle (°)	1.04	0.98	0.97	1.01
Total no. non-hydrogen atoms in AU	5,335	5,781	5,843	5,713
No. solvent molecules	65	333	393	173
B value, Wilson plot ($Å^2$)	41.18	39.73	33.51	43.79
Average B value ($Å^2$)	44.64	51.21	44.91	51.24
Ramachandran plot (%) (core, allowed, generous, disallowed)	84.7, 14.4, 0.5, 0.3	87.4, 10.2, 1.5, 0.8	88.4, 10.1, 1.2, 0.3	86.3, 11.9, 1.2, 0.7

[a] Data collection statistics from HKL log file.
[b] Refinement statistics from validation.

connecting β-strand 7 to β-strand 8 and α-helix 9 to α-helix 10 in the region specific to PRP4 at the bottom of the C-lobe as well as the final 8 amino acids at the C terminus, including the His_6 tag. Based on the electron density, Tyr^{849} at the end of the activation loop was modeled as phosphotyrosine. A total of 4 residues in the four discussed structures were found in disal-

lowed regions of the Ramachandran plot. With the exception of Thr[693] of chain A in the PRP4 + ADP complex, these residues (namely Arg[676] and Val[677] at the N terminus as well as Val[851] in the activation loop where flexibility renders proper modeling difficult) are located in regions of the protein that are not relevant to this publication. As for Thr[693] in the Gly-rich loop, the presence of ADP causes significant movement and sometimes decreases the quality of the electron density in that area, thus interfering with proper modeling. However, this residue is well defined and has good geometry in the x-ray structures of apo-PRP4 and PRP4-inhibitor complex.

PRP4 belongs to the CMGC (cyclin-dependent kinases, mitogen-activated protein kinases, glycogen synthase kinases, CDK-like kinases) group of the human kinome where it occupies a distinct branch within the DYRK family (34, 35). Other closely related kinases include CLKs, homeodomain-interact-

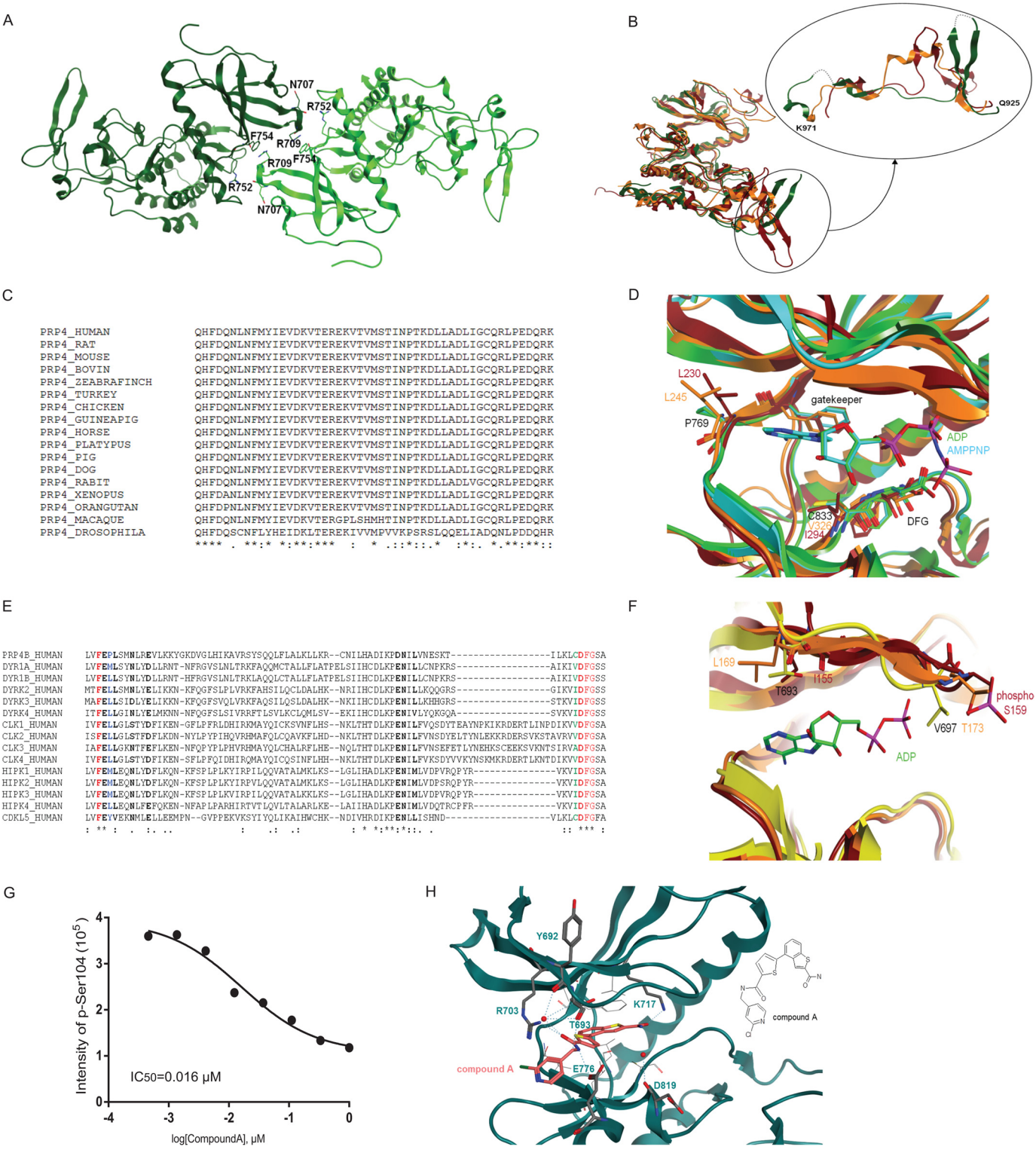

ing protein kinases, MSSK1, and SRPKs. Of these aforementioned kinases, the first x-ray structure to be reported in the public domain was that of SRPK1 in 2005 (36). Herein, we describe the first structures of PRP4. As shown in Fig. 5*A*, PRP4 x-ray crystal structures contain two molecules per asymmetric unit, namely chain A (in *light green*) and chain B (in *dark green*), that are connected by a 2-fold axis. Residues involved in potential H-bonds at the dimer interface are indicated. Because these two chains are similar in all structures described later, unless noted, our analysis focused on chain A of all structures. Of note, chain A also has a slightly better electron density around the glycine-rich loop compared with that of chain B in all structures solved.

To investigate the possibility of generating PRP4-specific inhibitors, we dissected structural differences between PRP4 and its closely related kinases, namely DYRK2 and CLK2, for which structural information is currently available. To this end, we superimposed the structures of PRP4 with those of apo-DYRK2 (Protein Data Bank code 3K2L) and small molecular mass-bound CLK2 (compound, (5*Z*)-5-(quinolin-6-ylmethylidene)-2-[(thiophen-2-ylmethyl)amino]-1,3-thiazol-4(5*H*)-one; Protein Data Bank code 3NR9). Subsequently, we calculated the overall root mean square deviation values for all main chains atoms in Molecular Operating Environment (Chemical Computing Group, Montreal, Canada) as 1.65 Å between apo-PRP4 chain A and DYRK2 chain A and 1.37 Å between apo-PRP4 chain A and CLK2 chain A (37). Although PRP4 displays a classical kinase fold, region 925–971 of PRP4 differs significantly in sequence and structure from the corresponding regions in DYRK2 and CLK2 (Fig. 5*B*; PRP4, *green*; CLK2, *orange*; DYRK2, *red*). In DYRK2, we observed two short antiparallel β-sheets with different lengths and orientations from the two long β-strands of PRP4. In CLK2, the corresponding region contains a small α-helix. Upon closer analysis, we found that although this region is highly conserved in PRP4 among species it does not appear to be homologous with other protein sequences in the human kinome and thus could play a role in PRP4-specific functions (Fig. 5*C*). Notably, a BLASTp search using the corresponding sequence (amino acids 925–971) failed to return any known structure.

We next examined the PRP4 structure at the ATP-binding site. Sequence alignment with the hinge region from several representatives of various protein kinase families revealed that the Pro^{769} of PRP4, which localizes 2 amino acids downstream of the gatekeeper (defined as the residue adjacent to the hinge and regulating the binding of nucleotides; the gatekeeper is Phe^{767} in the case of PRP4) and corresponds to Leu^{230} in DYRK2 and Leu^{245} in CLK2, is an unusual residue at this position within the hinge (Fig. 5, *D* and *E*; PRP4 + ADP, *green*; PRP4 + AMPPNP, *cyan*; DYRK2, *red*; CLK2, *orange*). Specifically, unlike the side chain of hydrophobic residues often found at this position, the Pro^{769} of PRP4 points toward the solvent and not toward the pocket, thus freeing some space at the hinge cleft. Another unique feature in PRP4 protein is that the Cys^{833} precedes the DFG motif. Among human kinases, this is an uncommon amino acid to be present at this position. For example, based on sequence and structure alignments, residues corresponding to Cys^{833} in kinases closely related to PRP4 are Val (Val^{326} in CLK2 and Val^{324} in CLK1a), Ile (Ile^{294} in DYRK2), and Ala (Ala^{319} in CLK3, Ala^{496} in SRPK1B, Ala^{529} in SRPK2A, and Ala^{540} in SRPK2B). However, CDKL5, like PRP4, also displays a Cys residue before the DFG motif and appears to be an exception in this group (Fig. 5, *D* and *E*). Taken together and given the renewed interest for irreversible inhibitors in the field of kinase modulators (38), the unusual Cys^{833} could be exploited to design covalent and selective PRP4 kinase modulators.

Next, by comparing the apo-, ADP-bound, and AMPPNP-bound PRP4 structures, we examined the flexibility of the Gly-rich loop (Fig. 5*F*; PRP4, *yellow*; DYRK2, *red*; CLK2, *orange*). Overall, the general binding mode of ADP and AMPPNP to PRP4 is similar to what has been observed in other kinases with the PRP4 hinge residues Glu^{768} and Leu^{770} forming two canonical hydrogen bonds with the adenosine ring despite constraints caused by Pro^{769}. However, the glycine-rich loop appears to display high plasticity. For example, in the apo-PRP4 x-ray structure, the Gly-rich loop is most ordered and can be entirely modeled. We observed that the tip of the loop is free to point back into the binding site, probably driven by the hydrophobicity of Phe^{698} side chain. On the other hand, in the ADP-bound PRP4 structure, the ADP β-phosphate forces Phe^{698} side chain to move away. As a consequence, the Gly-rich loop adopts a less rigid and more open conformation. Lastly, in the case of the AMPPNP-bound PRP4 structure, because of the additional γ-phosphate group, the Gly-rich loop is forced to adopt a completely open conformation with increasingly less order.

FIGURE 5. **PRP4 structural analysis.** *A*, content of asymmetric unit. Apo-PRP4 chain A is shown in *light green*, and chain B is shown in *dark green*. Residues involved in potential H-bonds at the dimer interface are shown. Arg^{752} side chain NH_2 and Phe^{754} main chain oxygen from one chain are involved with Asn^{707} main chain oxygen and Arg^{709} side chain NH_2 from the other. *B*, overall superposition between apo-PRP4 (*green*; B chain), CLK2 (*orange*), and DYRK2 (*red*). The PRP4 kinase fold is similar to these homologues (*left*) with the exception of the PRP4 region 925–971 (see *detail* shown in a different orientation). PRP4 residues 936–939 and 961–962 could not be built because of poor electron density and are thus modeled with *dashed lines*. *C*, multiple sequence alignment (ClustalW (40)) of human PRP4 region 925–971 with diverse PRP4 sequences shows very high sequence conservation. *D*, structural alignment between PRP4 + ADP (*green*), PRP4 + AMPPNP (*cyan*), DYRK2 (*red*), and CLK2 (*orange*) show significant differences at the hinge 2 residues downstream of the gatekeeper and in front of the DFG motif. *E*, multiple sequence alignment (ClustalW) of human PRP4 region encompassing the hinge and the DFG motif with the closest homologous kinase domains. Residues shown in *bold* are located within 4.5 Å of the ligand based on the PRP4 + AMPPNP complex (chain A). The gatekeeper and the DFG are shown in *red*. The gatekeeper +2 is shown in *blue*. Pro^{769} in PRP4 at this position is highly unusual. The residue preceding the DFG is shown in *green*. Cys^{833} in PRP4 at this position is unusual as well. *F*, structural alignment between apo-PRP4 (*yellow*), DYRK2 (*red*), and CLK2 (*orange*). Detail of the differences at the G-rich loop is shown. Note that although the entire protein backbone could be built, Gln^{695} and Val^{697} were modeled as alanine due to the lack of clear electron density for the side chains. *G*, inhibition of PAK4 phosphorylation by Compound A. The effect of Compound A on PRP4 kinase activity was evaluated in a PAK4 biochemical assay. The assay was performed as described under "Experimental Procedures." The PAK4 peptide harboring Ser^{104} was identified and quantified by Orbitrap mass spectrometry. IC_{50} was obtained by fitting data to a four-parameter logistic equation. *H*, potential interactions between PRP4 and Compound A. Potential hydrogen bonds are shown with *dashed lines*. Note that not all hydrogen bonds that involve water and are close to the hinge can take place simultaneously. Residues involved in such interactions are shown in *stick* representation. Protein residues involved in potential hydrophobic interactions with benzothiophene of Compound A are depicted. The two-dimensional structure of Compound A is illustrated on the *right* for clarity. *pSer*, phosphoserine.

Further inspection of the PRP4 Gly-rich loop also showed that PRP4 Thr^{693} is significantly different in both sequence and structure from its counterparts in other closely related kinases, such as Leu^{86} in SRPK1, Leu^{98} in SRPK2, Leu^{169} in CLK2, and Ile^{155} in DYRK2 (Fig. 5*F*). In addition, Val^{697} of PRP4 points straight down in the apo-PRP4 structure unlike its counterparts in DYRK2 (Ser^{159}) and CLK2 (Thr^{173}), which point away from the ATP-binding site (Fig. 5*F*).

To further explore the feasibility of generating more potent and selective PRP4 kinase inhibitors, a complex between PRP4 and Compound A was examined by co-crystallization. Compound A is a small molecule identified from a high throughput compound screen and shown to be active in MS-based biochemical assay using PAK4 as substrate (IC_{50} = 0.016 μM) (Fig. 5*G* and supplemental Table 5 for kinase selectivity study) but exhibits low cellular permeability (data not shown). As illustrated in Fig. 5*H*, this co-crystal structure at 2.25-Å resolution shows the PRP4 kinase domain in its active conformation with an intact salt bridge between conserved Lys^{717} and Glu^{732}. In addition, the DFG motif adopts an "in" conformation with Asp^{834} pointing to the active site. Here, the tip of the Gly-rich loop is well defined as the ligand does not push the Phe^{698} side chain away as in the AMPPNP complex. As shown by the co-crystal structure, the catalytic Lys^{717} and the end of the hinge are bridged by Compound A, which utilizes the oxygen of the carboxamide substituent at C2 of the benzothiophene scaffold as an H-bond acceptor for Lys^{717} (2.9 Å in distance between heavy atoms), whereas the NH_2 of this C2 carboxamide substituent forms a water-mediated H-bond with the main chain carbonyl oxygen of Asp^{819}. Compound A also forms a network of hydrogen bonds with the Gly-rich loop. For example, the carbonyl oxygen of the amide linker acts as an H-bond acceptor for the side chain NH_2 of Arg^{703} (2.7 Å in distance), and the same carbonyl oxygen may interact with the side chain NH_2 of Arg^{703} as well as the main chain oxygens of Tyr^{692} and Thr^{693} via a water molecule. Furthermore, the NH of the amide linker is also involved in hydrogen bonds formed with the side chain oxygens of Glu^{776} (2.9 and 3.2 Å in distance, respectively).

There are a number of aromatic and hydrophobic interactions present in this complex. First, the benzothiophene core of Compound A and PRP4 kinase Val^{701} form arene-hydrogen interactions, which point directly toward the fused ring system. Upon closer inspection, we observed that the benzothiophene lies in a hydrophobic part of the ATP binding pocket and is sandwiched by the side chains of Val^{701}, Ala^{715}, Leu^{751}, Leu^{822}, Cys^{833}, the aliphatic portion of catalytic Lys^{717}, and the phenyl ring of Phe^{767}. The only small hydrophilic patch in this area is created by the main chain of Leu^{770} at the hinge region.

Lastly, the observed binding mode contrasts with that of common "hinge binders," thus suggesting a possibility to design selective compounds within this series. It is also conceivable to take advantage of the unique sequence and structure of PRP4 kinase at the Gly-rich loop in the Thr^{693} area to improve the compound selectivity. Most interestingly, we found a number of PRP4 amino acid residues that are involved in interactions with Compound A but are not conserved within its closely related kinases and could be exploited for PRP4 inhibitor selectivity. These residues include Met^{772} (corresponds to His residues in SRPK1/2 and to Leu^{248} in CLK2), Glu^{776} (corresponds to Lys in SRPK1/2 and to Asp^{252} in CLK2), and Arg^{703} (corresponds to Leu in SRPK1/2). Although future mutagenesis studies will be required to conclusively define the mechanisms involved, collectively, the aforementioned description of the PRP4 kinase domain structure suggests a high probability of success in rationally designing low molecular mass inhibitors with both specificity and potency against PRP4 kinase.

DISCUSSION

Drug discovery is a lengthy process that requires significant investment of both time and resources. A thorough target validation prior to initiating a full scale drug discovery effort is essential to address whether the activity of a given target is required for the maintenance of cancer dependence and whether the strategy to identify and optimize novel therapeutic agents is in place. To help answer these questions, we sought to further investigate PRP4 kinase functions in regulating cell growth/viability and better understand the downstream targets and structural properties of PRP4. As a result of these efforts, we have uncovered unique features of PRP4 kinase in regard to both kinase domain structure and substrate specificity that may ultimately facilitate a better understanding of PRP4 biology.

PRP4 kinase is a large protein that possesses an RS domain at its N terminus. This domain serves as an essential platform for interaction with other RS domain-containing proteins. The potential significance of the PRP4 kinase adaptor function therefore cannot be overlooked. However, it is apparent from the data presented herein that the kinase activity of PRP4 is essential for the regulation of cancer cell growth and survival, indicating the potential interest of PRP4 as a therapeutic target in oncology.

In an attempt to rapidly identify physiological substrates of PRP4 kinase, we utilized a SILAC-based methodology followed by AIMS validation to filter through the candidate list. As a result of this effort, we identified 29 potential substrates with robust changes following PRP4 knockdown. In parallel, we performed a panoramic survey of the PRP4 interactome and intersected the prospective interacting partners with high confidence candidates from AIMS validation, thereby effectively narrowing down the number of potential substrates to 12. Subsequently, we established a physiologically relevant, quantitative, and robust cell-based assay utilizing mass spectrometry. Notably, we were successful in developing the cell-based MRM assay for PRP4 utilizing PAK4 phosphopeptide. Furthermore, the accompanying biochemical assay utilizing recombinant PAK4 as substrate yielded an alternative approach for *in vitro* characterization of PRP4 kinase activity. The Ser^{104} site on PAK4 has previously been documented in literature, although its precise functional relevance is unknown. It is worth noting that the N terminus of PAK4 (amino acids 65–175) is important for its RNA-dependent interaction with ribosomal and RNA-binding protein and for its role in regulating nucleocytoplasmic shuttling (39). One could speculate that the PRP4-mediated phosphorylation of Ser^{104} may be important in regulating the preceding aspects of PAK4 function, thus effectively linking PRP4 kinase to PAK4 signaling.

To facilitate our understanding of the PRP4 kinase domain in more detail, we turned to structural biology evaluation. To our knowledge, this is the first structural information ever reported for PRP4. The x-ray crystal structures described herein include the apo, ADP-, AMPPNP-, and Compound A-bound kinase domain of PRP4. Specifically, we established a robust and straightforward platform for purification and crystallization of human PRP4 kinase domain (see "Experimental Procedures") amenable to both co-crystallization and soaking of apo crystals. This is critical for efficient structural biology support during the drug discovery process because the ability to produce a high number of structures in complex with different ligands in a rapid fashion is essential for driving the optimization of selected chemical series.

The present x-ray crystal structure studies may reveal clues to PRP4 kinase substrate specificity. It appears that residues 925–971 of PRP4, although different in shape and length, are related to the mitogen-activated protein kinase insert in SRPK1. The SRPK1 mitogen-activated protein kinase insert forms a groove where a 9-mer peptide derived from the consensus motif of SRPK1 substrate is bound (36). It is likely that the groove formed in PRP4 at region 925–971 may also have a role in substrate binding, thus conveying PRP4 substrate specificity.

A close inspection of several regions within the PRP4 kinase domain reveals distinct features that may be important for generating potent and selective small molecular mass inhibitors. For example, Pro^{769} of PRP4 points toward the solvent, freeing some space at the hinge region that could be exploited to build selectivity. In addition, the Cys^{833} preceding the DFG motif of PRP4 is uncommon among kinases and can be a potential target for an irreversible covalent interaction. Other opportunities also exist for designing a compound capable of forming an H-bond with the Thr^{693} side chain or a hydrophobic interaction with Val^{697} because both residues are not conserved in kinases closely related to PRP4. Also, it may be possible to design compounds forming an H-bond with the Thr^{693} side chain of PRP4 and/or a hydrophobic interaction with Val^{697}, neither of which is conserved in SRPK1/2, CLK2, and DYRK2.

Compound A, for which we reported the co-crystal structure with PRP4, could be a good starting point to incorporate these hypotheses into a future medicinal chemistry effort. Using the aforementioned information along with virtual docking, one may be able to generate a potent and selective PRP4 inhibitor for future biological studies.

To conclude, we have identified new and interesting avenues for future development of PRP4 kinase inhibitors, including unique structural features of PRP4 and potential pharmacodynamic markers of PRP4 kinase activity. Moreover, we have extended the known functional network of downstream effectors of PRP4 kinase and now offer additional insights into PRP4 kinase biology. Future efforts will be focused on identifying and generating potent and selective PRP4 kinase inhibitors and assessing their utility in relevant preclinical models of cancer.

Acknowledgments—We thank Christopher Arendt and Asher Zilberstein for early contributions and Ying Zhang for help with PRP4 expression and purification.

REFERENCES

1. Rosenberg, G. H., Alahari, S. K., and Käufer, N. F. (1991) prp4 from *Schizosaccharomyces pombe*, a mutant deficient in pre-mRNA splicing isolated using genes containing artificial introns. *Mol. Gen. Genet.* **226,** 305–309
2. Kojima, T., Zama, T., Wada, K., Onogi, H., and Hagiwara, M. (2001) Cloning of human PRP4 reveals interaction with Clk1. *J. Biol. Chem.* **276,** 32247–32256
3. Dellaire, G., Makarov, E. M., Cowger, J. J., Longman, D., Sutherland, H. G., Lührmann, R., Torchia, J., and Bickmore, W. A. (2002) Mammalian PRP4 kinase copurifies and interacts with components of both the U5 snRNP and the N-CoR deacetylase complexes. *Mol. Cell. Biol.* **22,** 5141–5156
4. Montembault, E., Dutertre, S., Prigent, C., and Giet, R. (2007) PRP4 is a spindle assembly checkpoint protein required for MPS1, MAD1, and MAD2 localization to the kinetochores. *J. Cell Biol.* **179,** 601–609
5. Huang, B., Ahn, Y. T., McPherson, L., Clayberger, C., and Krensky, A. M. (2007) Interaction of PRP4 with Kruppel-like factor 13 regulates CCL5 transcription. *J. Immunol.* **178,** 7081–7087
6. Schwelnus, W., Richert, K., Opitz, F., Gross, T., Habara, Y., Tani, T., and Käufer, N. F. (2001) Fission yeast Prp4p kinase regulates pre-mRNA splicing by phosphorylating a non-SR-splicing factor. *EMBO Rep* **2,** 35–41
7. Kiger, A. A., Baum, B., Jones, S., Jones, M. R., Coulson, A., Echeverri, C., and Perrimon, N. (2003) A functional genomic analysis of cell morphology using RNA interference. *J. Biol.* **2,** 27
8. Bennett, E. M., Lever, A. M., and Allen, J. F. (2004) Human immunodeficiency virus type 2 Gag interacts specifically with PRP4, a serine-threonine kinase, and inhibits phosphorylation of splicing factor SF2. *J. Virol.* **78,** 11303–11312
9. Schneider, M., Hsiao, H. H., Will, C. L., Giet, R., Urlaub, H., and Lührmann, R. (2010) Human PRP4 kinase is required for stable tri-snRNP association during spliceosomal B complex formation. *Nat. Struct. Mol. Biol.* **17,** 216–221
10. Huang, Y., Deng, T., and Winston, B. W. (2000) Characterization of hPRP4 kinase activation: potential role in signaling. *Biochem. Biophys. Res. Commun.* **271,** 456–463
11. Alahari, S. K., Schmidt, H., and Käufer, N. F. (1993) The fission yeast prp4+ gene involved in pre-mRNA splicing codes for a predicted serine/threonine kinase and is essential for growth. *Nucleic Acids Res.* **21,** 4079–4083
12. Giroux, V., Iovanna, J., and Dagorn, J. C. (2006) Probing the human kinome for kinases involved in pancreatic cancer cell survival and gemcitabine resistance. *FASEB J.* **20,** 1982–1991
13. Schlabach, M. R., Luo, J., Solimini, N. L., Hu, G., Xu, Q., Li, M. Z., Zhao, Z., Smogorzewska, A., Sowa, M. E., Ang, X. L., Westbrook, T. F., Liang, A. C., Chang, K., Hackett, J. A., Harper, J. W., Hannon, G. J., and Elledge, S. J. (2008) Cancer proliferation gene discovery through functional genomics. *Science* **319,** 620–624
14. Ngo, V. N., Davis, R. E., Lamy, L., Yu, X., Zhao, H., Lenz, G., Lam, L. T., Dave, S., Yang, L., Powell, J., and Staudt, L. M. (2006) A loss-of-function RNA interference screen for molecular targets in cancer. *Nature* **441,** 106–110
15. Duan, Z., Weinstein, E. J., Ji, D., Ames, R. Y., Choy, E., Mankin, H., and Hornicek, F. J. (2008) Lentiviral short hairpin RNA screen of genes associated with multidrug resistance identifies PRP-4 as a new regulator of chemoresistance in human ovarian cancer. *Mol. Cancer Ther.* **7,** 2377–2385
16. Bauer, J. A., Ye, F., Marshall, C. B., Lehmann, B. D., Pendleton, C. S., Shyr, Y., Arteaga, C. L., and Pietenpol, J. A. (2010) RNA interference (RNAi) screening approach identifies agents that enhance paclitaxel activity in breast cancer cells. *Breast Cancer Res.* **12,** R41
17. Otwinowski, Z., and Minor, W. (1997) Processing of x-ray diffraction data collected in oscillation mode. *Methods Enzymol.* **276,** 307–326
18. Matthews, B. W. (1968) Solvent content of protein crystals. *J. Mol. Biol.* **33,** 491–497
19. Kantardjieff, K. A., and Rupp, B. (2003) Matthews coefficient probabilities: improved estimates for unit cell contents of proteins, DNA, and protein-nucleic acid complex crystals. *Protein Sci.* **12,** 1865–1871
20. Potterton, E., Briggs, P., Turkenburg, M., and Dodson, E. (2003) A graph-

ical user interface to the CCP4 program suite. *Acta Crystallogr. D Biol. Crystallogr.* **59,** 1131–1137
21. Winn, M. D., Ballard, C. C., Cowtan, K. D., Dodson, E. J., Emsley, P., Evans, P. R., Keegan, R. M., Krissinel, E. B., Leslie, A. G., McCoy, A., McNicholas, S. J., Murshudov, G. N., Pannu, N. S., Potterton, E. A., Powell, H. R., Read, R. J., Vagin, A., and Wilson, K. S. (2011) Overview of the CCP4 suite and current developments. *Acta Crystallogr. D Biol. Crystallogr.* **67,** 235–242
22. McCoy, A. J., Grosse-Kunstleve, R. W., Adams, P. D., Winn, M. D., Storoni, L. C., and Read, R. J. (2007) Phaser crystallographic software. *J. Appl. Crystallogr.* **40,** 658–674
23. Navaza, J. (2001) Implementation of molecular replacement in AMoRe. *Acta Crystallogr. D Biol. Crystallogr.* **57,** 1367–1372
24. Emsley, P., Lohkamp, B., Scott, W. G., and Cowtan, K. (2010) Features and development of Coot. *Acta Crystallogr. D Biol. Crystallogr.* **66,** 486–501
25. Brünger, A. T., Adams, P. D., Clore, G. M., DeLano, W. L., Gros, P., Grosse-Kunstleve, R. W., Jiang, J. S., Kuszewski, J., Nilges, M., Pannu, N. S., Read, R. J., Rice, L. M., Simonson, T., and Warren, G. L. (1998) Crystallography & NMR system: a new software suite for macromolecular structure determination. *Acta Crystallogr. D Biol. Crystallogr.* **54,** 905–921
26. Bricogne, G., Blanc, E., Brandl, M., Flensburg, C., Keller, P., Paciorek, W., Roversi, P., Sharff, A., Smart, O. S., Vonrhein, C., and Womack, T. O. (2011) *BUSTER*, Version 2.9.1, Global Phasing Ltd., Cambridge, UK
27. Rhodes, D. R., and Chinnaiyan, A. M. (2005) Integrative analysis of the cancer transcriptome. *Nat. Genet.* **37,** (suppl.) S31–S37
28. Wu, R., Dephoure, N., Haas, W., Huttlin, E. L., Zhai, B., Sowa, M. E., and Gygi, S. P. (2011) Correct interpretation of comprehensive phosphorylation dynamics requires normalization by protein expression changes. *Mol. Cell. Proteomics* **10,** M111.009654
29. Jaffe, J. D., Keshishian, H., Chang, B., Addona, T. A., Gillette, M. A., and Carr, S. A. (2008) Accurate inclusion mass screening: a bridge from unbiased discovery to targeted assay development for biomarker verification. *Mol. Cell. Proteomics* **7,** 1952–1962
30. Linding, R., Jensen, L. J., Ostheimer, G. J., van Vugt, M. A., Jørgensen, C., Miron, I. M., Diella, F., Colwill, K., Taylor, L., Elder, K., Metalnikov, P., Nguyen, V., Pasculescu, A., Jin, J., Park, J. G., Samson, L. D., Woodgett, J. R., Russell, R. B., Bork, P., Yaffe, M. B., and Pawson, T. (2007) Systematic discovery of *in vivo* phosphorylation networks. *Cell* **129,** 1415–1426
31. Lee, S. H., Sterling, H., Burlingame, A., and McCormick, F. (2008) Tpr directly binds to Mad1 and Mad2 and is important for the Mad1-Mad2-mediated mitotic spindle checkpoint. *Genes Dev.* **22,** 2926–2931
32. Wells, C. M., and Jones, G. E. (2010) The emerging importance of group II PAKs. *Biochem. J.* **425,** 465–473
33. Ackermann, B. L., and Berna, M. J. (2007) Coupling immunoaffinity techniques with MS for quantitative analysis of low-abundance protein biomarkers. *Expert Rev. Proteomics* **4,** 175–186
34. Hanks, S. K., and Hunter, T. (1995) Protein kinases 6. The eukaryotic protein kinase superfamily: kinase (catalytic) domain structure and classification. *FASEB J.* **9,** 576–596
35. Manning, G., Whyte, D. B., Martinez, R., Hunter, T., and Sudarsanam, S. (2002) The protein kinase complement of the human genome. *Science* **298,** 1912–1934
36. Ngo, J. C., Chakrabarti, S., Ding, J. H., Velazquez-Dones, A., Nolen, B., Aubol, B. E., Adams, J. A., Fu, X. D., and Ghosh, G. (2005) Interplay between SRPK and Clk/Sty kinases in phosphorylation of the splicing factor ASF/SF2 is regulated by a docking motif in ASF/SF2. *Mol. Cell* **20,** 77–89
37. Group, C. C. (2011) *Molecular Operating Environment*, Chemical Computing Group, Montreal, Canada
38. Singh, J., Petter, R. C., Baillie, T. A., and Whitty, A. (2011) The resurgence of covalent drugs. *Nat. Rev. Drug. Discov.* **10,** 307–317
39. Baldassa, S., Calogero, A. M., Colombo, G., Zippel, R., and Gnesutta, N. (2010) N-terminal interaction domain implicates PAK4 in translational regulation and reveals novel cellular localization signals. *J. Cell. Physiol.* **224,** 722–733
40. Larkin, M. A., Blackshields, G., Brown, N. P., Chenna, R., McGettigan, P. A., McWilliam, H., Valentin, F., Wallace, I. M., Wilm, A., Lopez, R., Thompson, J. D., Gibson, T. J., and Higgins, D. G. (2007) Clustal W and Clustal X version 2.0. *Bioinformatics* **23,** 2947–2948